

**OXIDE FILM CHARACTERISTICS UNDER PWR PRIMARY COOLANT  
CONDITIONS**



Angkana Luttikul

A Thesis Submitted in Partial Fulfilment of the Requirements  
for the Degree of Master of Science  
The Petroleum and Petrochemical College, Chulalongkorn University  
in Academic Partnership with  
The University of Michigan, The University of Oklahoma,  
Case Western Reserve University and Institut Français du Pétrole  
2010

530023

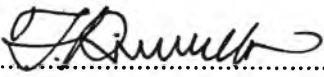
**Thesis Title:** Oxide Film Characteristics under PWR Primary Coolant  
Conditions  
**By:** Angkana Luttikul  
**Program:** Petrochemical Technology  
**Thesis Advisors:** Assoc. Prof. Thirasak Rirksomboon  
Prof. Derek H. Lister  
Prof. Frank R. Steward

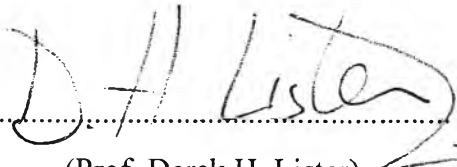
---

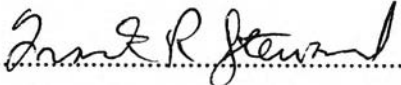
Accepted by the Petroleum and Petrochemical College, Chulalongkorn  
University, in partial fulfilment of the requirements for the Degree of Master of  
Science.


  
..... Dean  
(Asst. Prof. Pomthong Malakul)

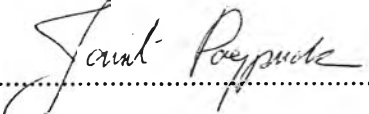
**Thesis Committee:**

  
.....  
(Assoc. Prof. Thirasak Rirksomboon)

  
.....  
(Prof. Derek H. Lister)

  
.....  
(Prof. Frank R. Steward)

  
.....  
(Assoc. Prof. Pramoch Rangsunvigit)

  
.....  
(Dr. Janit Pongpuak)

**ABSTRACT**

5171001063: Petrochemical Technology Program  
Angkana Luttikul: Oxide Film Characteristics under PWR Primary  
Coolant Conditions  
Thesis Advisors: Assoc. Prof. Thirasak Rirksomboon, Prof. Derek H.  
Lister, and Prof. Frank R. Steward, 201 pp.  
Keywords: Crud-Induced Power Shift/ Alloy 600/ Alloy690/Alloy 800/  
Corrosion Product/ Heat Treatment/ Oxide Film

In pressurized water reactors (PWRs), the deposition of corrosion products (crud) on the fuel cladding surface causes Crud-Induced Power Shift (CIPS), which shifts the neutron flux distribution. Since corrosion products found on the cladding are rich in Ni, the Ni-based alloy steam generator (SG) tubing is the primary concern for corrosion product inventory that has led to the development of CIPS. This study was carried out to study the effects of SG alloy composition and heat treatment, boron concentration and zinc addition on oxide film formation under PWR primary coolant conditions. The corrosion tests were performed on specimens of Alloy 600, Alloy 690, Alloy 800, 304 stainless steel and Zirc-4 in an autoclave (titanium autoclave and stainless steel autoclave), simulating PWR primary coolant conditions. After exposure for several days, the oxides on the samples were characterized with several techniques. The results revealed that nickel-based alloys and SS304 were covered with Fe-rich crystallites overlaying an amorphous Cr-rich layer, while Zircaloy-4 was covered with a ZrO<sub>2</sub> layer. For the same heat treatment, the higher-Cr alloys apparently produced more protective oxide (finer and more compact crystallites) than the lower-Cr alloys. The heat treatment effects were observed on all alloys, but were overshadowed by effects of alloy composition. The compactness of the oxide films was strongly boron dependent; the compact oxides were formed in the coolant containing boron. In addition, the oxides on Ni-based alloys and SS304 seem to be more protective by the addition of 20 ppb Zn in the coolant.

## บทคัดย่อ

อังคณา ลัทธิกุล : การศึกษาลักษณะของออกไซด์ที่เกิดขึ้นภายใต้สภาวะของน้ำหล่อเย็นในเตาปฏิกรณ์นิวเคลียร์แบบน้ำความดันสูง (Oxide Film Characteristics under PWR Primary Coolant Conditions) อาจารย์ที่ปรึกษา : รศ.ดร. ชีรศักดิ์ ฤกษ์สมบูรณ์, ศ.ดร. ดีเรค เอช ลิสเตอร์ และ ศ.ดร. แฟรงค์ อาร์ สจีวิต, 201 หน้า

ในเตาปฏิกรณ์นิวเคลียร์แบบน้ำความดันสูง การสะสมของอนุภาคออกไซด์บนผิวหน้าแลกเปลี่ยนความร้อนในแกนของเตาปฏิกรณ์นิวเคลียร์เป็นสาเหตุให้เกิดความผิดปกติในการทำงานของแกนในเตาปฏิกรณ์ พบว่าอนุภาคของออกไซด์ส่วนใหญ่ที่สะสมบนผิวหน้าแลกเปลี่ยนความร้อนในแกนของเตาปฏิกรณ์นิวเคลียร์เป็นนิเกิลออกไซด์ซึ่งเกิดมาจากการกัดกร่อนของโลหะผสมนิเกิลที่ใช้ทำเป็นท่อแลกเปลี่ยนความร้อนในเครื่องผลิตไอน้ำ ดังนั้นท่อแลกเปลี่ยนความร้อนเหล่านี้จึงเป็นแหล่งกำเนิดที่สำคัญของอนุภาคออกไซด์ที่จะนำไปสู่การเกิดความผิดปกติในการทำงานของแกนในเตาปฏิกรณ์ การทดลองนี้ศึกษาผลกระทบจากองค์ประกอบที่แตกต่างกันของโลหะผสมนิเกิล, กระบวนการบำบัดโลหะด้วยความร้อน (Heat Treatment) บนโลหะผสมนิเกิลที่แตกต่างกัน, การใช้สารละลายที่มีความเข้มข้นของโบรอนแตกต่างกัน และการเติมสารละลายสังกะสีต่อการเกิดออกไซด์ภายใต้สภาวะของน้ำหล่อเย็นในเตาปฏิกรณ์นิวเคลียร์แบบน้ำความดันสูง ในการทดลอง ตัวอย่างของโลหะผสมนิเกิลที่มีองค์ประกอบต่างกัน (Alloy 600, Alloy 690 and Alloy 800), เหล็ก (304 stainless steel) และ โลหะผสมของเซอร์โคเนียม (Zircaloy-4) ได้ถูกใส่เข้าไปในภาชนะที่ทนต่ออุณหภูมิและความดันสูง (Autoclave) เพื่อให้เกิดการกัดกร่อนในน้ำที่จำลองสภาวะของน้ำหล่อเย็นดังกล่าวเป็นเวลาหลายวัน หลังจากนั้นได้ทำการวิเคราะห์ออกไซด์ที่เกิดขึ้นบนชิ้นตัวอย่างด้วยเครื่องมือวิเคราะห์ทางพื้นผิวหลายประเภท ผลการศึกษาพบว่าออกไซด์ที่เกิดขึ้นบนโลหะผสมนิเกิลและบนเหล็กมีลักษณะเป็นออกไซด์สองชั้นที่ประกอบขึ้นด้วยชั้นผลึกของเหล็กออกไซด์บนชั้นของโครเมียมออกไซด์ ในขณะที่ออกไซด์ที่เกิดขึ้นบนโลหะผสมของเซอร์โคเนียมเป็นเซอร์โคเนียมออกไซด์เพียงชั้นเดียว ความแข็งแรงของออกไซด์ที่เกิดขึ้นบนโลหะผสมนิเกิลเพิ่มขึ้นตามปริมาณของโครเมียมที่เป็นองค์ประกอบอยู่ในโลหะผสมนิเกิล โลหะผสมนิเกิลที่ผ่านกระบวนการบำบัดโลหะด้วยความร้อนที่ต่างกันก่อให้เกิดออกไซด์ที่ต่างกัน อย่างไรก็ตามผลกระทบจากองค์ประกอบของโลหะผสมนิเกิลต่อการเกิดออกไซด์บนโลหะผสมนิเกิลเห็นได้ชัดเจนกว่าผลกระทบจากกระบวนการบำบัดโลหะด้วยความร้อน โบรอนเป็นปัจจัยสำคัญในการเกิดออกไซด์ที่แน่นและแข็งแรง นอกจากนี้ยังพบว่า

การเติมสารละลายสังกะสีช่วยให้ออกไซด์ที่เกิดขึ้นบนโลหะผสมนิกเกิลและบนเหล็กมีความ  
แข็งแรงมากขึ้น

## ACKNOWLEDGEMENTS

I would like to thank the Petroleum and Petrochemical College and the National Center of Excellence for Petroleum, Petrochemicals, and Advanced Materials, Thailand for giving me an opportunity to study a master's degree and giving me a full scholarship, which covered the tuition fee.

My research work would not be completed well without the assistance and support of people in Thailand and in Canada. Thus, I would like to acknowledge the assistance and support of people who have cooperated in this research.

First of all, I would like to thank to my advisors, Prof. Derek H. Lister, Prof. Frank R. Steward and Assoc. Prof. Thirasak Rirksomboon for giving me an opportunity to carry out my research at University of New Brunswick, Canada. It gave me a lot of valuable experience that I have never gotten before.

The valuable guidance, the intensive support, patience and the endless help throughout this research work of Prof. Derek H. Lister will never be forgotten. My research work cannot be completed without his assistance. I am very appreciative of all his advice and it is my honor to have him as my advisor.

Next, I would like to extend my special thanks to Mr. Piti Srisukvatananan for teaching me many things from his experience and for all good advice and technical supports throughout this research work, which made my work here easier. Mr. Andrew Feicht is thankful for all good advice and technical supports as well.

Further, I would like to thank Dr. Lihui Liu, Dr. Suporn Boonsue, Dr. Louise Weaver, Mr. Steven Cogswell and Dr. Douglas Hall for helping me analyse my samples and giving me useful information and suggestions about my results.

Without the following persons, I could not have the samples for my research work, Keith Rollins and Aden Briggs, who cut all samples in this work for me.

Moreover, I would like to give a special thanks to Prof. Frank R. Steward and his wife (Jacky) who have helped and taken care of me during I stayed in Canada and to P'Naid, P'Pit, P'Kate, R'Suporn, R'Justin and all Thai students for their friendship, standing beside me and cheering me up. I will never forget our times in every events, trips and parties.

Finally, I would like to give my deepest gratitude to my beloved family in Thailand for their unconditional love, blessing, constant encouragement and cheering me up.

## TABLE OF CONTENTS

	<b>PAGE</b>
Title Page	i
Abstract (in English)	iii
Abstract (in Thai)	iv
Acknowledgements	vi
Table of Contents	viii
List of Tables	xii
List of Figures	xvi
Abbreviations	xxiii
<b>CHAPTER</b>	
<b>I INTRODUCTION</b>	<b>1</b>
<b>II LITERATURE REVIEW</b>	<b>4</b>
2.1 Pressurized Water Reactor (PWR)	4
2.1.1 Materials of PWR Primary Coolant Loop	5
2.1.2 PWR Primary Coolant Chemistry	8
2.2 Corrosion of Materials	9
2.2.1 Definition of Corrosion	9
2.2.2 Oxide Film Formation	10
2.3 Heat Treatment	14
2.3.1 Definition of Heat Treatment	14
2.3.2 Objectives of Heat Treatment	14
2.3.2.1 Annealing	15
2.3.2.2 Hardening	17
2.3.3 Heat Treatment of Nickel Alloys	18
2.3.3.1 Mill Annealing (MA)	18
2.3.3.2 Thermal Treatment (TT)	18
2.4 Crud Induced Power Shift (CIPS)	19
2.4.1 The Causes of CIPS	19



<b>CHAPTER</b>		<b>PAGE</b>
	2.4.2 Effect of Solubility of Crud	22
	2.4.3 Effect of Heat Flux of Fuel Element	23
	2.4.4 Mitigation Strategies for CIPS or AOA	23
	2.4.4.1 Adding Zinc	24
	2.4.4.2 Operating the Plant at an Elevated pH	24
	2.4.4.3 Using Enriched Boric Acid	24
	2.4.4.4 Cleaning Fuel Assemblies	25
	2.5 Zinc Addition	25
<b>III</b>	<b>EXPERIMENTAL</b>	28
	3.1 Materials	28
	3.2 Equipment	28
	3.2.1 Experimental Loop	29
	3.2.2 Test Sections and Specimens	29
	3.2.2.1 Static Ti-2 Autoclave with Heat Transfer	30
	3.2.2.2 Static Ti-2 Autoclave without Heat Transfer	32
	3.2.2.3 Static Stainless Steel Autoclave without Heat Transfer	34
	3.3 Methodology	35
	3.3.1 Experimental Procedure	35
	3.3.2 Coolant Chemistry	36
	3.3.3 Oxide Characterization	36
	3.3.3.1 EDX and SEM Analyses	37
	3.3.3.2 SIMS Analysis	38
	3.3.3.3 XPS Analysis	38
	3.3.4 Test Matrix	39

CHAPTER	PAGE
<b>IV RESULTS AND DISCUSSION</b>	<b>42</b>
4.1 Corrosion Tests in Ti-2 Autoclave with Heat	
Transfer	42
4.1.1 Run 1	42
4.1.1.1 EDX and SEM Analyses	44
4.1.1.2 SIMS Analysis	49
4.1.1.3 XPS Analysis	52
4.1.2 Run 2	56
4.1.2.1 EDX and SEM Analyses	58
4.1.3 Run 3	64
4.1.3.1 EDX and SEM Analysis	66
4.1.3.2 XPS Analysis	70
4.2 Corrosion Tests in Ti-2 Autoclave without Heat	
Transfer	78
4.2.1 Run 4	78
4.2.1.1 EDX and SEM Analyses	81
4.2.2 Run 5	101
4.2.2.1 EDX and SEM Analyses	104
4.2.3 Run 6	120
4.2.3.1 EDX and SEM Analyses	123
4.2.4 Run 7	127
4.2.4.1 EDX and SEM Analyses	130
4.3 Corrosion Tests in SS Autoclave without Heat	
Transfer	137
4.3.1 Run 8	137
4.3.1.1 EDX and SEM Analyses	140
4.3.2 Run 9	152
4.3.2.1 EDX and SEM Analyses	155

<b>CHAPTER</b>	<b>PAGE</b>
4.4 Discussion	170
4.4.1 Oxide Morphology	170
4.4.2 Effect of SG Alloy Composition	171
4.4.3 Effect of SG Alloy Heat Treatment	171
4.4.4 Effect of Boron Concentration	172
4.4.5 Effect of Zn Addition	173
4.4.6 Effect of Dissolved Ions in the Coolant	174
4.4.7 Effect of Exposure Time	175
4.4.8 Effect of Coolant Temperature	175
<b>V CONCLUSIONS AND RECOMMENDATIONS</b>	<b>177</b>
5.1 Conclusions	177
5.2 Recommendations	177
<b>REFERENCES</b>	<b>179</b>
<b>APPENDICES</b>	<b>187</b>
<b>Appendix A</b> XPS data	187
<b>Appendix B</b> Coolant Preparation	192
<b>Appendix C</b> LRS Spectra	196
<b>Appendix D</b> Calculation of Corrosion Rate	199
<b>CURRICULUM VITAE</b>	<b>200</b>

## LIST OF TABLES

TABLE	PAGE
2.1 Material construction of each component in primary coolant loop	5
2.2 Chemical composition of Alloy 600, Alloy 690 and Alloy 800 (weight %)	6
2.3 Coolant chemistry conditions	9
2.4 Net lattice energies of some spinels (Lister, 1994)	27
2.5 Site preference energies of certain cations (Miller, 1959)	27
3.1 Supplied SG tubes	28
3.2 Comparison of heat fluxes and boiling rate in this experiment with plant data	32
3.3 Coolant chemistry conditions	36
3.4 Test matrix	40
4.1 Weight of the sample bands before and after exposure in Run 1	43
4.2 Coolant chemistry before and after exposure in Run 1	43
4.3 EDX result from the convex surface of SG1 in Run 1	45
4.4 EDX result on the cross-sectional surface along radial lines of SG1 in Run 1	46
4.5 EDX analyses on the convex surface of SS304 in Run 1	48
4.6 EDX analyses on the convex surface Zircaloy-4 in Run 1	48
4.7 Compositions of Zircaloy-4 and SS304	50
4.8 Quantitative XPS analysis of oxide film grown on SG3 in Run 1 (at.%)	56
4.9 Weight of the sample bands before and after exposure in Run 2	57
4.10 EDX result from the convex surface of SG2 and SG3 in Run 2	59
4.11 EDX analyses on the convex surface of SS304 in Run 2	61
4.12 EDX analyses on the convex surface of Zirc-4 in Run 2	63
4.13 Comparison of Zirc-4 corrosion rate between Run 1 and Run 2	63
4.14 Weight of the sample bands before and after exposure in Run 3	64
4.15 Coolant chemistry before and after exposure in Run 3	65
4.16 EDX result from the convex surface of SG3 in Run 3	66

TABLE	PAGE
4.17 EDX analyses on the convex surface of SS304 in Run 3	68
4.18 EDX analyses on the convex surface of Zirc-4 in Run 3	69
4.19 Corrosion rates of Zirc-4 in Run 1, Run 2 and Run 3	70
4.20 Possible oxides on SS304 surface before sputtering in Run 3	71
4.21 Quantitative XPS analysis of oxide film grown on SS304 in Run 3 before sputtering (at.%)	72
4.22 Weight of the samples before and after exposure in Run 4	79
4.23 Coolant chemistry before and after exposure in Run 4	81
4.24 EDX result from the convex surface of Alloy 600 MA in Run 4	84
4.25 EDX result from the convex surface of Alloy 600 TT in Run 4	85
4.26 EDX result from the convex surface of Alloy 690 MA from Valinox in Run 4	89
4.27 EDX result from the convex surface of Alloy 690 TT from Valinox in Run 4	89
4.28 EDX result from the convex surface of Alloy 690 CD from Valinox in Run 4	90
4.29 EDX result from the convex surface of Alloy 800 MA in Run 4	92
4.30 EDX result from the convex surface of Alloy 800 SP in Run 4	92
4.31 Ni and Fe ratio in crystallite on Alloy 600, Alloy 690 and Alloy 800 in Run 4	93
4.32 EDX result on the cross-sectional surface along radial lines of Alloy 600 MA in Run 4	96
4.33 EDX result from the convex surface of SS304-1 in Run 4	97
4.34 EDX result from the convex surface of SS304-5 in Run 4	98
4.35 EDX result from the surface of Zirc-4 in Run 4	100
4.36 Comparison of Zirc-4 corrosion rate between Run 3 and Run 4	100
4.37 Weight of the samples before and after exposure in Run 5	102
4.38 Coolant chemistry before and after exposure in Run 5	104
4.39 EDX result from the convex surface of Alloy 600 MA in Run 5	106
4.40 EDX result from the convex surface of Alloy 600 TT in Run 5	106

TABLE	PAGE
4.41 EDX result from the convex surface of Alloy 690 MA in Run 5	109
4.42 EDX result from the convex surface of Alloy 690 TT in Run 5	109
4.43 EDX result from the convex surface of Alloy 690 CD in Run 5	109
4.44 EDX result from the convex surface of Alloy 800 MA in Run 5	111
4.45 EDX result from the convex surface of Alloy 800 SP in Run 5	112
4.46 EDX result from the convex surface of SS304-4 in Run 5	114
4.47 EDX result from the convex surface of SS304-5 in Run 5	114
4.48 EDX result from the surface of Zirc-4 in Run 5	115
4.49 Comparison of Zirc-4 corrosion rate between Run 4 and Run 5	120
4.50 Weight of the samples before and after exposure in Run 6	122
4.51 Coolant chemistry before and after exposure in Run 6	123
4.52 EDX result from the convex surface of Alloy 600 MA in Run 6	124
4.53 EDX result from the convex surface of SS304 in Run 6	126
4.54 EDX result from the convex surface of Zirc-4 in Run 6	127
4.55 Weight of the samples before and after exposure in Run 7	129
4.56 Coolant chemistry before and after exposure in Run 7	130
4.57 EDX result from the convex surface of Alloy 600 MA in Run 7	132
4.58 EDX result from the convex surface of SS304 in Run 7	133
4.59 EDX result from the convex surface of Zirc-4 in Run 7	135
4.60 Corrosion rates of Zirc-4 in Run 2, Run 6 and Run 7	137
4.61 Weight of the samples before and after exposure in Run 8	139
4.62 Coolant chemistry before and after exposure in Run 8	140
4.63 EDX result from the convex surface of Alloy 600 MA in Run 8	142
4.64 EDX result from the convex surface of Alloy 600 TT in Run 8	142
4.65 EDX result from the convex surface of Alloy 690 MA in Run 8	144
4.66 EDX result from the convex surface of Alloy 690 TT in Run 8	145
4.67 EDX result from the convex surface of Alloy 690 CD in Run 8	145
4.68 EDX result from the convex surface of Alloy 800 MA in Run 8	147
4.69 EDX result from the convex surface of Alloy 800 SP in Run 8	147
4.70 EDX result from the convex surface of SS304-4 in Run 8	149

<b>TABLE</b>	<b>PAGE</b>
4.71 EDX result from the convex surface of SS304-8 in Run 8	150
4.72 EDX result from the surface of Zirc-4 in Run 8	151
4.73 Comparison of Zirc-4 corrosion rate between Run 4 and Run 8	152
4.74 Weight of the samples before and after exposure in Run 9	154
4.75 Coolant chemistry before and after exposure in Run 9	155
4.76 EDX result from the convex surface of Alloy 600 MA in Run 9	158
4.77 EDX result from the convex surface of Alloy 600 TT in Run 9	158
4.78 EDX result from the convex surface of Alloy 690 MA in Run 9	161
4.79 EDX result from the convex surface of Alloy 690 TT in Run 9	161
4.80 EDX result from the convex surface of Alloy 690 CD in Run 9	161
4.81 EDX result from the convex surface of Alloy 800 MA in Run 9	163
4.82 EDX result from the convex surface of Alloy 800 SP in Run 9	163
4.83 EDX result from the convex surface of SS304-2 in Run 9	166
4.84 EDX result from the convex surface of SS304-3 in Run 9	166
4.85 EDX result from the convex surface of Zirc-4 in Run 9	167
4.86 Comparison of Zirc-4 corrosion rate between Run 8 and Run 9	171
4.87 Corrosion rate of Zirc-4 in Run 1, 2, 6 and 7	174
A.1 XPS survey signals of SG3 in Run 1	188
A.2 Ni 2p <sub>3/2</sub> core-level signals of SG3 in Run 1	188
A.3 Cr 2p <sub>3/2</sub> core-level signals of SG3 in Run 1	189
A.4 Ti 2p core-level signals of SG3 in Run 1	189
A.5 O 1s core-level signals of SG3 in Run 1	190
A.6 C 1s core-level signals of SG3 in Run 1	190
C.1 Raman shift of crystallites on SG alloy samples in Run 4	196

## LIST OF FIGURES

FIGURE		PAGE
1	SEM image of Crud found on the cladding (Hawkes, 2004).	2
2.1	Schematic of Pressurized Water Reactor (PWR) ( <a href="http://www.cleansafeenergy.org">http://www.cleansafeenergy.org</a> ).	5
2.2	Schematic cross-section through magnetite film on carbon steel (Lister <i>et al.</i> , 2001).	11
2.3	Schematic of the formation mechanism of the magnetite film on the steel surface in high temperature water (Cheng and Steward, 2004).	11
2.4	Schematic cross-section through oxide film on stainless steel in PWR primary piping (Lister and Venkateswaran, 1995).	13
2.5	Schematic cross-section through oxide film on Alloy 600 & Alloy 800 in PWR & PHWR primary circuits (Lister and Venkateswaran, 1995).	14
2.6	Solubility of different borate species (Bouaziz, 1961).	21
2.7	Venn diagram of suspected AOA causes (Hawkes, 2004).	22
3.1	A schematic diagram of the experimental loop.	29
3.2	Configuration of Ti-2 autoclave with the circulating water.	30
3.3	SG sample number assignment and autoclave lid assembly.	31
3.4	Schematic of specimens in autoclave without heat transfer.	33
3.5	Configuration of static Ti-2 autoclave (without the circulating water).	34
3.6	Configuration of static stainless steel autoclave (without the circulating water).	35
3.7	Schematic of SG sample and locations of analyses in Runs 1-3.	37
3.8	Schematic of samples and locations of analyses in Runs 4-9.	37
3.9	Magnified schematic of sectioned SG sample and locations of analyses.	38
4.1	SG1 sample band in Run 1 (a) before exposure and (b) after exposure.	42
4.2	SEM cross-section image of oxide film grown on SG1 in Run 1 at the 30° position (facing the heater); (a) at low magnification (b) at higher magnification.	45



FIGURE	PAGE
4.3 SEM images of (a) SG3 and (b) SG6 in Run 1.	47
4.4 SEM images of (a) SS304 and (b) Zirc-4 in Run 1.	48
4.5 SIMS analysis on Zircaloy-4 in Run 1.	49
4.6 SIMS analysis on SG3 in Run 1.	51
4.7 SIMS analysis on SG6 in Run 1.	51
4.8 SIMS analysis on SS304 in Run 1.	52
4.9 XPS depth profile on SG3 (-15°) in Run 1.	53
4.10 Ni 2p <sub>3/2</sub> core level spectra of oxide film grown on SG3 in Run 1.	53
4.11 Cr 2p <sub>3/2</sub> core level spectra of oxide film grown on SG3 in Run 1.	54
4.12 Fe 2p core level spectra of oxide film grown on SG3 in Run 1.	55
4.13 Ti 2p core level spectra of oxide film grown on SG3 in Run 1.	55
4.14 SG3 sample band in Run 2 (a) before exposure and (b) after exposure.	57
4.15 Photographs of SG sample bands (a) SG3 in Run 2 and (b) SG1 in Run 1.	57
4.16 SEM images of (a) SG2 and (b) SG3 in Run 2.	59
4.17 SEM images of SS304 in Run 2 (a and b) and in Run 1 (c and d).	61
4.18 SEM image of Zirc-4 in Run 2.	62
4.19 Comparison of surface morphologies of Zirc-4 in Run 1 (a) with Zirc-4 in Run 2 (b).	63
4.20 SG3 sample band in Run 3 (a) before exposure and (b) after exposure.	64
4.21 SEM image of SG3 in Run 3.	67
4.22 SEM image of SS304 in (a) Run 1 and (b) Run 3.	68
4.23 SEM image of Zirc-4 in Run 3.	69
4.24 Magnified SEM image of small crystal on Zirc-4 surface in Run 3.	69
4.25 Ni 2p <sub>3/2</sub> core level spectra of oxide film grown on SS304 as function of sputtering (Run 3).	73
4.26 Fe 2p <sub>3/2</sub> core level spectra of oxide film grown on SS304 as function of sputtering (Run 3).	74
4.27 Cr 2p <sub>3/2</sub> core level spectra of oxide film grown on SS304 as function of sputtering (Run 3).	75

FIGURE	PAGE
4.28 Ti 2p <sub>3/2</sub> core level spectra of oxide film grown on SS304 as function of sputtering (Run 3).	75
4.29 Zn 2p <sub>3/2</sub> core level spectra of oxide film grown on SS304 as function of sputtering (Run 3).	76
4.30 O 1s core level spectra of oxide film grown on SS304 as function of sputtering (Run 3).	76
4.31 Samples after exposure in Run 4.	78
4.32 SEM images of Alloy 600 MA (a and b) and Alloy 600 TT (c and d).	83
4.33 Schematic of a carbide precipitation (a time-temperature-transformation, TTT) diagram for Inconel 600 (Scarberry <i>et al.</i> , 1976).	84
4.34 Comparison of SEM images of Alloy 600 TT in Run 3 (a) with Alloy 600 TT in Run 4 (b).	85
4.35 SEM images of Alloy 690 MA in Run 4.	87
4.36 SEM images of Alloy 690 TT from Sandvik (a) and Valinox (b) in Run 4.	87
4.37 SEM images of Alloy 690 CD in Run 4.	88
4.38 SEM images of Alloy 690 MA, TT and CD in Run 4.	88
4.39 SEM images of Alloy 800 MA (a and b) and Alloy 800 SP (c and d) in Run 4.	91
4.40 SEM images of Alloy 600 MA, Alloy 690 MA and Alloy 800 MA in Run 4.	94
4.41 Comparison of the surface morphologies of Alloy 600 TT with Alloy 690 TT in Run 4.	95
4.42 SEM cross-section image of oxide film grown on Alloy 600 MA in Run 4.	96
4.43 SEM images of SS304-1 (a and b) and SS304-5 (c and d) in Run 4.	97
4.44 Comparison of the surface morphologies of SS304 in Run 3 (a) with SS304 in Run 4 (b).	98
4.45 SEM images of Zirc-4 in Run 4.	99

<b>FIGURE</b>	<b>PAGE</b>
4.46 Comparison of the surface morphologies of Zirc-4 in Run 3 (a) with Zirc-4 in Run 4 (b).	100
4.47 Samples after exposure in Run 5.	101
4.48 SEM images of Alloy 600 MA (a and b) and Alloy 600 TT (c and d) in Run 5.	105
4.49 SEM images of Alloy 690 MA from Valinox (a), Alloy 690 CD from Valinox (b), Alloy 690 TT from Sandvik (c) and Alloy 690 TT from Valinox (d) in Run 5.	108
4.50 Comparison of SEM images of Alloy 690 TT, MA and CD from Valinox in Run 5.	108
4.51 SEM images of Alloy 800 MA (a and b) and Alloy 800 SP (c and d) in Run 5.	111
4.52 Comparison of SEM images of Alloy 600 MA, Alloy 690 MA and Alloy 800 MA in Run 5.	112
4.53 Comparison of SEM images of Alloy 600 TT and Alloy 690 TT in Run 5.	113
4.54 SEM images of SS304-4 and SS304-5 in Run 5.	114
4.55 SEM images of Zirc-4 in Run 5.	115
4.56 Comparison of the surface morphologies of Alloy 600 MA (a) and Alloy 600 TT (c) in Run 4 with Alloy 600 MA (b) and Alloy 600 TT (d) in Run 5.	117
4.57 Comparison of the surface morphologies of Alloy 690 TT, MA and CD in Run 4 (top) with Alloy 690 TT, MA and CD in Run 5 (below).	118
4.58 Comparison of the surface morphologies of Alloy 800 MA (a) and Alloy 800 SP (c) in Run 4 with Alloy 800 MA (b) and Alloy 800 SP (d) in Run 5.	119
4.59 Comparison of the surface morphologies of SS304 in Run 4 (a) with SS304 in Run 5 (b).	119
4.60 Comparison of the surface morphologies of Zirc-4 in Run 4 (a) with Zirc-4 in Run 5 (b).	120

<b>FIGURE</b>	<b>PAGE</b>
4.61 Samples before (left) and after (right) exposure in Run 6.	121
4.62 SEM images of Alloy 600 MA in Run 6.	124
4.63 SEM images of SS304 in Run 6.	125
4.64 Comparison of the surface morphologies of SS304 in Run 6 (a) with SS304 in Run 3 (b).	126
4.65 SEM images of Zirc-4 in Run 6.	127
4.66 Samples before (left) and after (right) exposure in Run 7.	128
4.67 SEM images of Alloy 600 MA in Run 7.	131
4.68 Comparison of the surface morphologies of Alloy 600 MA in Run 6 (a) with Alloy 600 MA in Run 7 (b).	132
4.69 Comparison of the surface morphologies of SS304 in Run 6 (a) with SS304 in Run 7 (b).	133
4.70 Comparison of the surface morphologies of SS304 in Run 2 (a) with SS304 in Run 7 (b).	134
4.71 SEM images of Zirc-4 in Run 7.	135
4.72 Comparison of the surface morphologies of Zirc-4 in Run 6 (a) with Zirc-4 in Run 7 (b).	136
4.73 Samples after exposure in Run 8.	138
4.74 SEM images of Alloy 600 MA (a) and Alloy 600 TT (b) in Run 8.	141
4.75 SEM images of Alloy 690 MA from Valinox (a), Alloy 690 CD from Valinox (b), Alloy 690 TT from Sandvik (c) and Alloy 690 TT from Valinox (d) in Run 8.	143
4.76 Comparison of SEM images of Alloy 690 MA, TT and CD from Valinox in Run 8.	144
4.77 SEM images of Alloy 800 MA (a and b) and Alloy 800 SP (c and d) in Run 8.	146
4.78 Comparison of SEM images of Alloy 600 MA (a and d), Alloy 690 MA (b and e) and Alloy 800 MA (c and f) in Run 8.	148
4.79 Comparison of SEM images of Alloy 600 TT and Alloy 690 TT in Run 8.	148

<b>FIGURE</b>	<b>PAGE</b>
4.80 SEM images of SS304-4 and SS304-8 in Run 8.	149
4.81 SEM images of Zirc-4 in Run 8.	150
4.82 Comparison of surface morphologies of Alloy 800 MA in Run 4 (a) with Alloy 800 MA in Run 8 (b).	151
4.83 Comparison of the surface morphologies of Zirc-4 in Run 4 (a) with Zirc-4 in Run 8 (b).	152
4.84 Samples after exposure in Run 9.	153
4.85 SEM images of Alloy 600 MA (a and b) and Alloy 600 TT (c and d) in Run 9.	157
4.86 SEM images of Alloy 690 MA from Valinox (a), Alloy 690 CD from Valinox (b), Alloy 690 TT from Sandvik (c) and Alloy 690 TT from Valinox (d) in Run 9.	160
4.87 Comparison of SEM images of Alloy 690 MA, TT and CD from Valinox in Run 9.	160
4.88 SEM images of Alloy 800 MA (a and b) and Alloy 800 SP (c and d) in Run 9.	162
4.89 Comparison of SEM images of Alloy 600 MA, Alloy 690 MA and Alloy 800 MA in Run 9.	164
4.90 Comparison of SEM images of Alloy 600 TT and Alloy 690 TT in Run 9.	165
4.91 SEM images of SS304-2 and SS304-3 in Run 9.	165
4.92 SEM images of Zirc-4 in Run 9.	167
4.93 Comparison of the surface morphologies of Alloy 600 MA (a) and Alloy 600 TT (b) in Run 8 with Alloy 600 MA (c) and Alloy 600 TT (d) in Run 9.	168
4.94 Comparison of the surface morphologies of Alloy 690 MA, TT and CD in Run 8 (top) with Alloy 690 MA, TT and CD in Run 9 (below).	169
4.95 Comparison of the surface morphologies of Alloy 800 MA (a) and Alloy 800 SP (c) in Run 8 with Alloy 800 MA (b) and Alloy 800 SP (d) in Run 9.	170

FIGURE	PAGE
4.96 Comparison of the surface morphologies of SS304 in Run 8 (a) with SS304 in Run 9 (b).	170
4.97 Comparison of the surface morphologies of Zirc-4 in Run 8 (a) with Zirc-4 in Run 9 (b).	171
A.1 XPS survey spectrum of SG3 in Run 1.	187
A.2 O 1s core level spectra of SG3 in Run 1.	190
A.3 C 1s core level spectra of SG3 in Run 1.	191
A.4 XPS survey spectra of SS304 before sputtering in Run 3.	191
C.1 Raman spectra of crystallites on SG alloy samples in Run 4.	196
C.2 Raman spectra of $\text{Ni}_{0.5}\text{Fe}_{2.5}\text{O}_4$ .	197
C.3 Raman spectra of $\text{Ni}_{0.67}\text{Fe}_{2.33}\text{O}_4$ .	197
C.4 Raman spectra of $\text{NiFe}_2\text{O}_4$ .	198

**ABBREVIATIONS**

AOA	Axial Offset Anomaly
BE	Binding Energy
CD	Cold Drawing
CIPS	Crud-Induced Power Shift
CPS	Count Per Second
EBA	Enriched Boric Acid
EDX	Electron Dispersive X-ray spectroscopy
ICP-OES	Inductively-Couple Plasma-Optical Emission Spectroscopy
IGSCC	Intergranular Stress Corrosion Cracking
MA	Mill Annealing
mdd	mg/(dm <sup>2</sup> .day)
PWR	Pressurized Water Reactor
PWSCC	Primary Water Stress Corrosion Cracking
SCC	Stress Corrosion Cracking
SEM	Scanning Electron Microscope
SG	Steam Generator
SIMS	Secondary Ion Mass Spectrometry
SNB	Sub-cooled Nucleate Boiling
SP	Shot Peening
SS304	304 Stainless Steel
TT	Thermal Treatment
XPS	X-ray Photoelectron Spectroscopy
Zirc-4	Zircaloy-4